https://doi.org/10.37434/tpwj2020.12.01

IMPACT OF TECHNOLOGICAL PARAMETERS OF ARC DEPOSITION OF AN ANTICORROSION LAYER IN THE VESSEL OF WWER-1000 REACTOR ON RESIDUAL STRESS DISTRIBUTION

O.V. Makhnenko and **O.S. Kostenevych**
E.O. Paton Electric Welding Institute of the NAS of Ukraine
11 Kazymyr Malevych Str., 03150, Kyiv, Ukraine. E-mail: office@paton.kiev.ua

Substantiation of extension of safe operating life of the vessels of WWER-1000 reactors in service requires taking into account the residual stresses, arising during fabrication as a result of heating at welding or surfacing heating and their redistribution after heat treatment. Automatic submerged-arc surfacing with strip electrodes was used for the cylindrical part of the vessels, and manual coated electrode arc surfacing was applied for the nozzle zone surface (internal surface of nozzles Dn850 and their fillets), as well as other difficult-of-access places of the vessel. The process and parameters of the mode of anticorrosion arc surfacing can markedly influence the microstructural phase composition of the HAZ of base material, 15Kh2NMFA vessel steel, as well as residual stress distribution. Mathematical modeling was used for prediction of microstructural phase transformations in the HAZ, at deposition of the protective anticorrosion layer, based on experimental welding thermokinetic diagram of austenite decomposition of 15Kh2NMFA steel, and distribution of residual stresses in WWER-1000 reactor vessel was derived, allowing for microstructural transformations at different technological modes of arc surfacing. Comparison of the results on residual stress distribution after deposition and heat treatment at different technological modes showed the presence of the zone of compressive stresses, which arise in the HAZ of 15Kh2NMFA steel, as a result of martensite-bainite transformation. 24 Ref., 6 Tables, 15 Figures.

K e y w o r d s : reactor vessel, WWER-1000, anticorrosion arc surfacing, heat-treatment, residual stresses, microstructural phase transformations, mathematical modeling, thermokinetic diagram, 15Kh2NMFA steel

The majority of nuclear power reactors in Ukraine belong to WWER-1000 type, where the vessel is made from thick-walled forged shells from low-alloy high-strength steel of 15Kh2NMFA grade, which are joined by circumferential welds. For corrosion protection the internal surface of the vessel is coated with an anticorrosion layer from austenitic material.

At present the most important scientific-engineering task is extension of safe operating life of the reactor vessels (RV) in service. Its substantiation requires taking into account the residual stresses (RS) arising as a result of heating at welding or surfacing, and their redistribution after heat treatment. Technological parameters of anticorrosion arc surfacing can greatly influence the microstructural phase composition of the heat-affected zone (HAZ) of base material of 15Kh2NMFA vessel steel, as well as residual stress distribution.

In accordance with normative documentation requirements [1], automatic submerged-arc surfacing with a welding strip (the main recommended method), or manual coated electrode arc surfacing or argon-arc surfacing should be used for deposition of anticorrosion coatings on the reactor vessel. In keeping with manufacturing plant documentation [2], automatic submerged-arc surfacing with strip electrodes was used for the RV cylindrical part, and manual coated electrode arc surfacing was applied for the nozzle zone surface (internal surface of nozzles Dn850 and their fillets), as well as for other difficult-of-access places.

RV anticorrosion surfacing was performed in two layers: first layer from austenitic material with increased content of chromium and nickel, Sv-07Kh25N13, second layer also from an austenitic material Sv-04Kh20N10G2B (Sv-08Kh19N10G2B), ensuring the general thickness of the deposited layer of 9 mm [1, 2]. Manual arc surfacing was performed with coated electrodes ZIO-8 (first layer) and EA-898/21B (second layer).

Technological parameters for automatic submerged-arc surfacing (OF-10) with strip electrodes were as follows: [1, 3–6]: current I_w = 600–750 A, voltage U_a = 32–36 V, strip electrode width b = 40–60 mm, preheating and concurrent heating temperature T_h = 100–250 °C, deposition rate v_d = 7–10 m/h; for manual coated electrode arc surfacing [1, 7, 8]: current I_w = 130–150 A, voltage U_a = 26–30 V, 4–5 mm dia electrodes, preheating and concurrent

O.V. Makhnenko — https://orcid.org/0000-0002-8583-0163, O.S. Kostenevych — https://orcid.org/0000-0002-7427-2805

Table 1. Chemical composition of 15Kh2NMFA steel, wt.% [10]

C	Si	Mn	Cr	Ni	Mo	Cu	S	P	V	As	Co
0.13–0.18	0.13–0.37	0.3–0.6	1.8–2.3	1.0–1.5	0.5–0.7	<0.3	<0.02	<0.02	0.10–0.12	<0.04	<0.03

heating temperature T_h = 100–250 °C, deposition rate v_d = 3 m/h.

After processing of the internal surface RV was subjected to heat treatment by high-temperature tempering mode for residual stress relaxation. Maximum heat treatment (HT) temperature could reach 610 °C [2, 6], 620 °C [2, 5], 650–670 °C [1, 9] and soaking duration could be from 5 to 20 h.

Composition of RV base material of 15Kh2NMFA steel (Table 1) was to meet the requirements of TU 108-765–78 [10]. Thermophysical and physicomechanical properties of base material and deposit material are given in [11, 12], depending on temperature.

The work provides comparative analysis of the results of calculations to determine the microstructural phase composition and mechanical properties of the HAZ of RV base material, as well as distribution of residual stresses at different technological modes of anticorrosion surfacing and subsequent heat treatment. The influence of technological parameters of arc surfacing on residual stress distribution was studied, using finite-element model of the nozzle zone of WWER-1000 RV, which includes characteristic sections of surfacing the VR cylindrical part and internal surface of nozzles Dn850 (Figure 1).

Modeling was performed assigning the following technological modes (Table 2): for automatic submerged-arc surfacing of the nozzle zone cylindrical shell, variation of strip electrode width b and preheating temperature T_{pr}, as well as soaking duration at heat treatment was performed. For the internal surface of nozzles Dn850, including the fillets, manual coated electrode arc welding at the nominal mode was modeled.

Two models of surfacing heating source were applied: strip — for automatic submerged-arc surfacing of RV cylindrical shell and spot (or normal-circular), simulating manual coated electrode arc surfacing of the internal surface of nozzle Dn850, as well as the fillets.

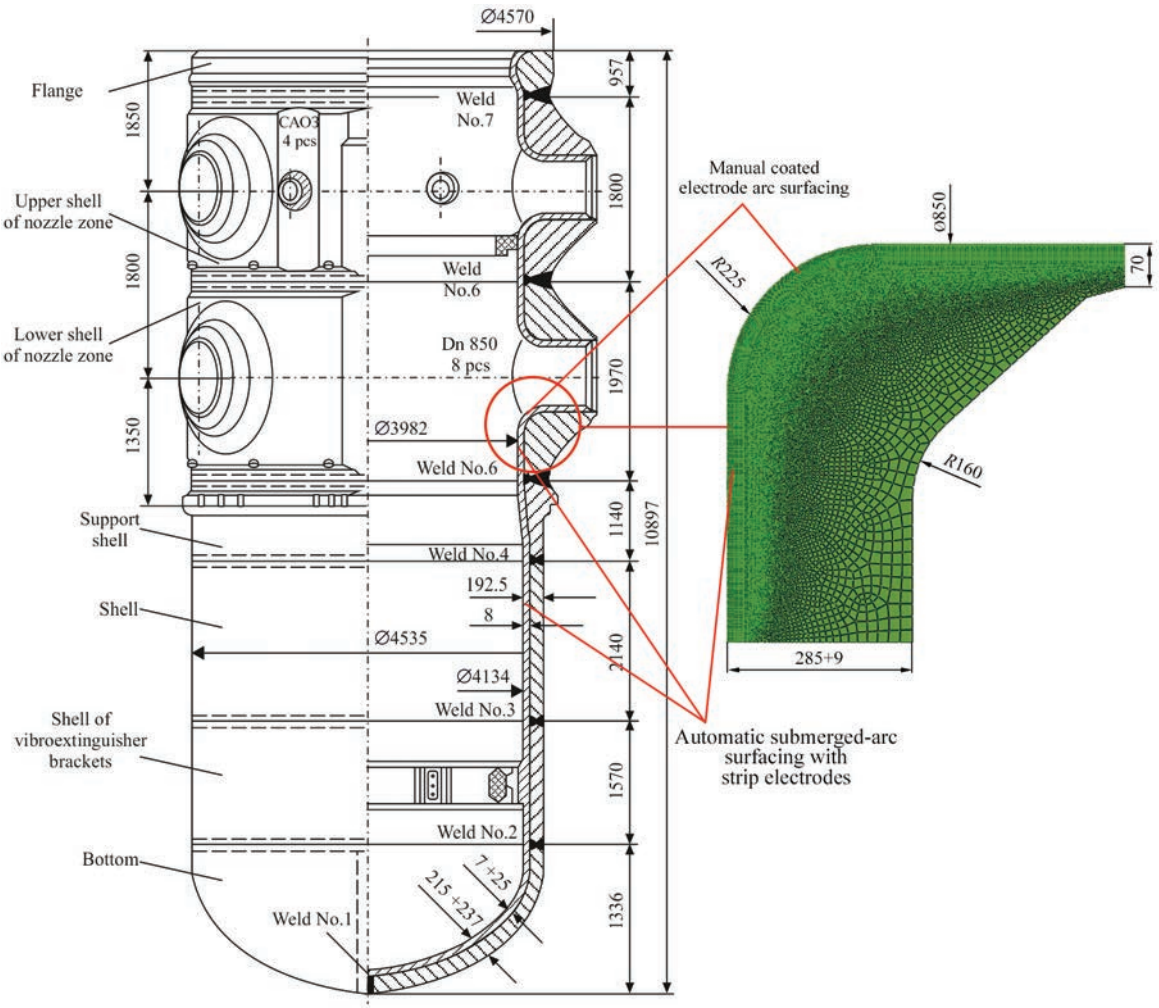

Figure 1. Schematic of location of the zones of manual and automatic surfacing of WWER-1000 RV with an anticorrosion layer and finite-element model of the nozzle zone [1, 2]

Table 2. Modes of arc surfacing and HT assumed in calculations

Current I_w, A	Voltage U_a, V	Efficiency coefficient η	Effective heat input, kJ/mm	Deposition rate v_d, mm/s	Bead width b, mm	Preheating temperature T_{pr}, °C	Soaking time at HT, h (T = 650 °C)
Manual coated electrode arc surfacing							
150	30	0.75	4.066	0.83	15	250	20
150	30	0.75	4.066	0.83	15	250	10
150	30	0.75	4.066	0.83	15	250	5
Automatic submerged-arc surfacing with strip electrodes							
650	32	0.9	9.360	2.0	40	250	20
700	32	0.9	14.608	1.4	60	150	20
700	32	0.9	14.608	1.4	60	250	20
700	32	0.9	14.608	1.4	60	250	10
700	32	0.9	14.608	1.4	60	250	5

Table 3. Results of calculation of HAZ size and cooling rates at different technological parameters of surfacing

Bead width b, mm	Preheating temperature T_{pr}, °C	FZ depth, mm	HAZ depth in base material, mm	Cooling rate w (800–500 °C), °C/s
15 (manual surfacing)	250	1	7	8–11
40	250	1	9	4–5
60	250	1	10	3–4
60	150	1	8	5–7

The problem of nonstationary heat conductivity in arc surfacing was solved in a two-dimensional definition with the assumption of a fast moving heat source and axial symmetry at sequential deposition of surfacing passes with step-by-step tracing in time from the start of heating of metal in each deposited pass to cooling to the temperature of concurrent heating. Distribution of thermal power of strip source W_1 and point source W_2 in the two-dimensional definition in a cylindrical system of coordinates can be represented by the respective dependencies (1) and (2) [13]:

$$W_1(r,z,t) = \frac{2Q\sqrt{K_r K_z}}{\pi v_h t_h \left[1+\sqrt{\frac{K_z}{\pi}}b\right]} \times \exp\left[-K_r(r-r_0)^2 - K_z(z-z_0)^2\right]; \quad (1)$$

$$W_2(r,z,t) = \frac{2Q\sqrt{K_r K_z}}{\pi v_h t_h} \times \exp\left[-K_r(r-r_o)^2 - K_z(z-z_o)^2\right], \quad (2)$$

where r, z are the coordinates (radial and axial) of the considered RV point; r_0, z_0 are the coordinates of the center of moving heat source; K_r, K_z are the concentration coefficients of the specific heat flow; t_h is the heating time; Q is the effective power of the heat source ($Q = \eta I_w U_a$); η is the coefficient of heat source efficiency; v_d is the deposition rate; b is the strip electrode width.

Derived calculation results of maximum temperature distributions and characteristic thermal cycles at deposition allowed evaluation of the dimensions of the fusion zone (FZ) and HAZ, as well as cooling rate

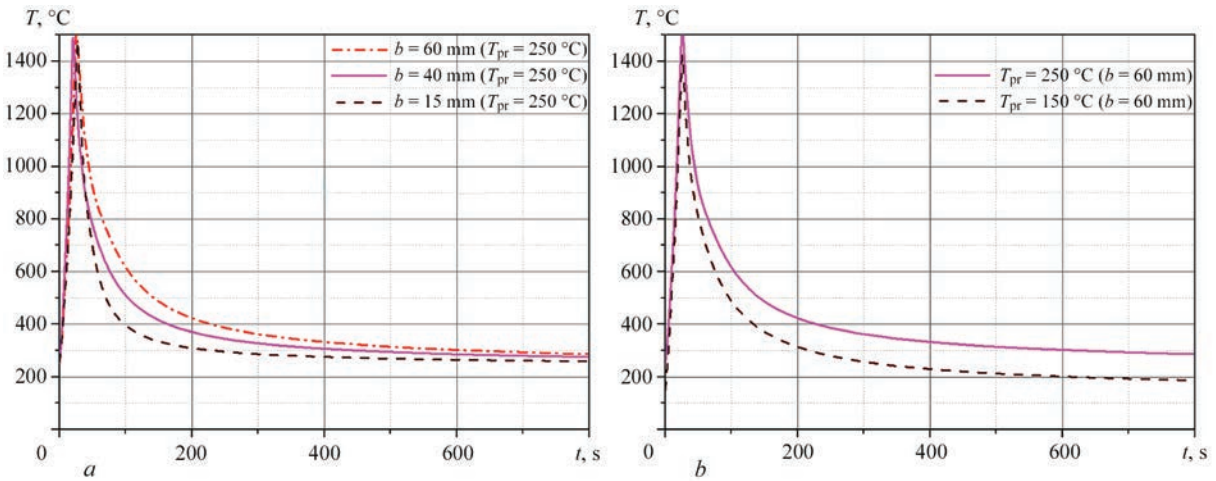

Figure 2. Characteristic thermal cycles at variation of: *a* — bead width; *b* — preheating temperature, T_{pr}

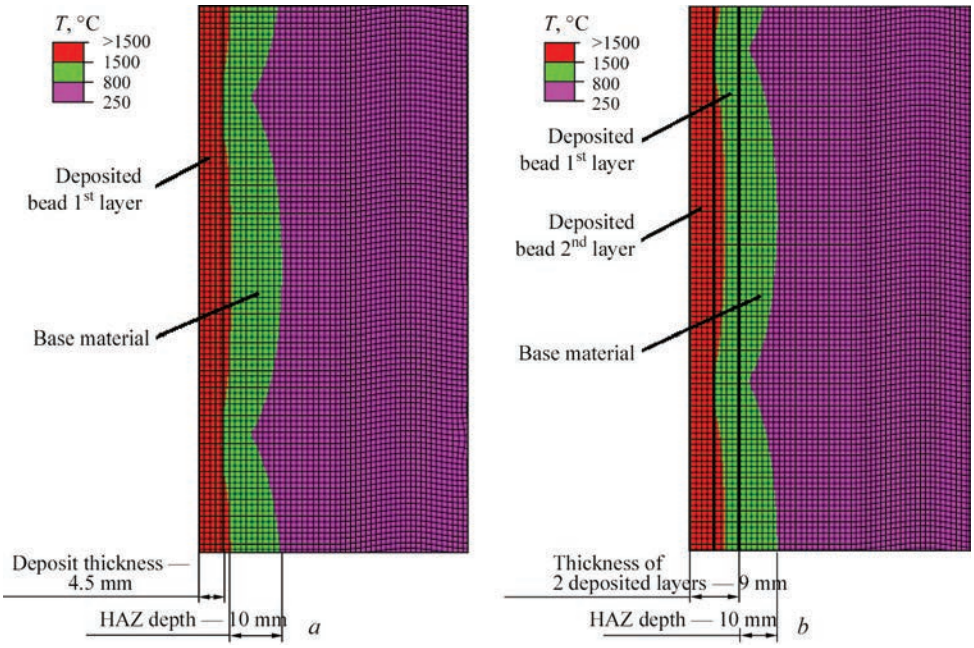

Figure 3. Characteristic dimensions of FZ (T > 1500 °C) and HAZ (1500 °C > T> 800 °C) for submerged-arc surfacing with strip electrodes of: *a* — first layer; *b* — second layer

of the metal in reactor vessel surfaced zones at different technological modes (Figure 2, Table 3). Results were obtained for different bead widths b: at automatic arc surfacing with strip electrodes — 40, 60 mm, at manual coated electrode arc welding — 15 mm, and at different preheating temperatures T_{pr} for automatic surfacing that are equal to 150 and 250 °C.

From the viewpoint of microstructural transformations, important is the size (depth) of the HAZ in base material. As after the second deposited layer the HAZ shifts by the value of the first layer width, the depth of the HAZ in base material is actually determined as a result of deposition of the first layer. One can see by the results (Table 3, Figure 2) that the minimum HAZ size in base material (up to 7 mm depth) and maximum rate of HAZ metal cooling in the temperature range of 800–500 °C (8–11 °C/s) were derived for manual coated electrode arc surfacing of nozzle Dn850. Rather high cooling rate (5–7 °C/s) was obtained for arc surfacing with strip electrode of width b = 60 mm at preheating temperature of 150 °C. The lowest cooling rate (3–4 °C/s) and the greatest depth of the HAZ in base material (up to 10 mm) were obtained for the mode of arc surfacing with strip electrode at b = 60 mm and preheating temperature of 250 °C (Figure 3).

FZ chemical composition can differ essentially from that of the filler material, as a result of mixing with the base metal. In keeping with [7], the mixing ratio g_0 (%), namely the fraction of base metal in the deposited metal depends on the deposition mode and is determined as follows:

$$g_0 = \frac{F_{BM}}{F_{BM} + F_d} 100\ \%, \qquad (3)$$

where F_0 is the cross-sectional area of molten base metal; F_d is the cross-sectional area of the deposited metal.

Microstructural phase composition in FZ taking into account the mixing of base and filler metal, can be approximately determined according to Schaeffler structural diagram [14] based on the values of equivalent nickel and chromium:

$$\begin{pmatrix} Ni_{eq} = \%\,Ni + 30 \cdot \%\,C + 0.5 \cdot \%\,Mn \\ Cr_{eq} = \%\,Cr + \%\,Mo + 1.5 \cdot \%\,Si + 0.5 \cdot \%\,Nb \end{pmatrix}. \qquad (4)$$

Results of calculation of mixing ratio and approximate microstructural phase composition in the FZ, according to Schaeffler diagram, are given in Table 4 at increase of the heat input from the nominal value by 10, 20, 30, 40 %.

Calculation of microstructural phase composition, according to Schaeffler diagram [14] for different FZ regions at essential deviations of the heat input values from the nominal one, showed that in terms of formation of an austenitic structure in FZ, 30 % increase of the heat input is a critical value for automatic submerged-arc surfacing with strip electrode and 40 % increase is a critical value for manual coated electrode arc surfacing. This is indicative of reliable formation of austenitic structure in the FZ (up to 5–10 % content of ferrite) at nominal values of the heat input. At mathematical modeling of temperature distributions, it was found that the critical value of the mixing ratio,

Table 4. Determination of mixing ratios at heat input variation

Increase of heat input against nominal value, %	Area of deposited bead, mm²	Area of molten base metal, mm²	Mixing ratio g_0, %	Ni_{eq}	Cr_{eq}	Austenite in FZ, %
0	180 (automatic submerged-arc surfacing with strip electrode b = 40 mm)	26	13	14.7	22.5	90–95
10		52	23	13.7	20.3	95–100
20		86	32	12.8	18.1	100
30		110	38	12.2	16.8	a+m+f
0	67 (manual coated electrode arc surfacing	13	16	14.3	21.7	90–95
10		21	23	13.7	20.2	95–100
20		27	28	13.2	19.0	95–100
30		36	35	12.5	17.6	100
40		43	39	12.1	16.6	a+m+f

Table 5. Numerical data from TKD of austenite decomposition in 15Kh2NMFA steel under characteristic thermal cycle of welding/surfacing conditions

Cooling rate w_j, °C/s	Transformation temperatures at cooling stage, °C				Bainite V_b/martensite V_m fraction, %	Hardness $HV1$, kgf/mm²
	B_s	B_f	M_s	M_f		
3	485	315	343	315	98/2	383
4	478	343	343	280	80/20	380
5	468	425	425	298	10/90	426

non-exceeding which ensures formation of the austenitic structure in the FZ, is equal to g_0 = 38–39 % at nominal values of g_0 = 13–16 % (Table 4). Therefore, further mathematical modeling of microstructural phase composition, mechanical properties and stress-strain state in RV surfaced zone did not take into account the filler material mixing with base metal in the FZ or the change of chemical composition of austenitic deposit material.

Modeling of microstructural phase transformations in low-alloy steel HAZ during welding or surfacing can be performed using the approach based on application of parametric (regression) equations derived at PWI [15, 16]. In this work, mathematical modeling of microstructural transformations in the HAZ of 15Kh2NMFA steel was performed with application of thermokinetic diagram (TKD) of austenite decomposition for characteristic welding/surfacing cycles exactly for 15Kh2NMFA steel. For this purpose, physical modeling of microstructural transformations in the HAZ of RV base material at arc surfacing in Gleeble3800 unit, and metallographic analysis of 15Kh2NMFA steel samples were performed [13]. Physical modeling results are presented in [13] in the form of two plotted TKD of austenite decomposition for characteristic cycles of welding/surfacing at different cooling rates w_j in the temperature range of 800–500 °C and at different maximum heating temperatures (1000 and 1350 °C). For convenience of mathematical modeling of microstructural transformations in the HAZ of 15Kh2NMFA steel, the welding TKD of austenite decomposition, averaged relative to maximum heating temperature, which is proposed in [17], was used. It is plotted for different cooling rates w_j in the characteristic temperature range of 800–500 °C (Figure 4, Table 5).

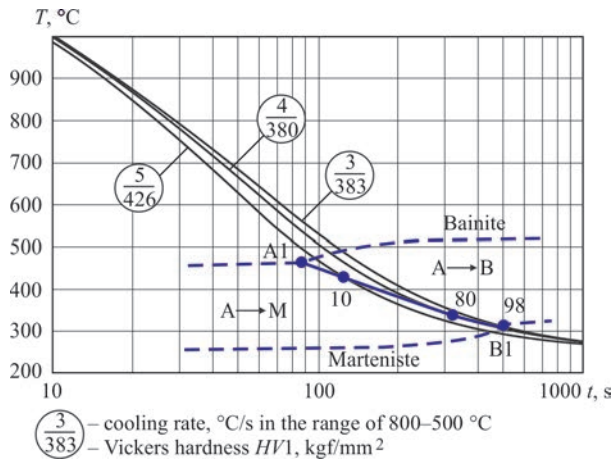

Figure 4. Thermokinetic diagram of austenite decomposition in 15Kh2NMFA steel for characteristic cooling cycles at welding [17]

The numerical data of TKD of 15Kh2NMFA steel [17] (Table 5) allow deriving the interpolation dependencies for all the TKD parameters (temperature of the start of bainite B_s and martensite transformation M_s, finish of bainite B_f and martensite transformation M_f, maximum fraction of martensite $V_{m.max}$ and $V_{b.max}$) for intermediate cooling rates w.

It was experimentally established that the initial microstructure of samples from 15Kh2NMFA steel is bainite with a small fraction of martensite of up to 3–5 % (Figure 5). Hardness of Vickers samples is $HV1$ = 315–325 kgf/mm² (3150–3250 MPa). Bainite grain size is 15–20 μm (8–9 grain size number to ASTM). Experimental data are in good agreement

with the available data [18, 19] as to the initial microstructural state of 15Kh2NMFA steel.

Figures 6 and 7 show the derived results of calculation of the weight fraction of each microstructural phase during surfacing and in the final microstructure of base material HAZ after cooling, according to numerical data of 15Kh2NMFA steel TKD.

Calculated data according to Figure 6, obtained on the base of experimental TKD of austenite decomposition in 15Kh2NMFA steel showed that heating at submerged-arc surfacing with strip electrodes (b = = 60 mm) resulted in formation of a small fraction of martensite of up to 15 % at preheating temperature T_{pr} = 250 °C (cooling rate of 3–4 °C/s) and formation of a predominant content of 90 % martensite in the final microstructure at preheating temperature T_{pr} = = 150 °C (cooling rate of 5–7 °C/s) (Figure 6).

Comparison of the results for the two values of strip electrode width (Figure 7) at anticorrosion surfacing showed that at the width b = 40 mm the fraction of martensite formed in the HAZ is 70–90 %, and at the width of b = 60 mm — it is up to 15 % martensite. At manual coated electrode arc surfacing (b = = 15 mm) martensite content in the final microstructure after cooling is equal to 90 %.

Results of mathematical modeling of microstructural phase composition of 15Kh2NMFA steel HAZ

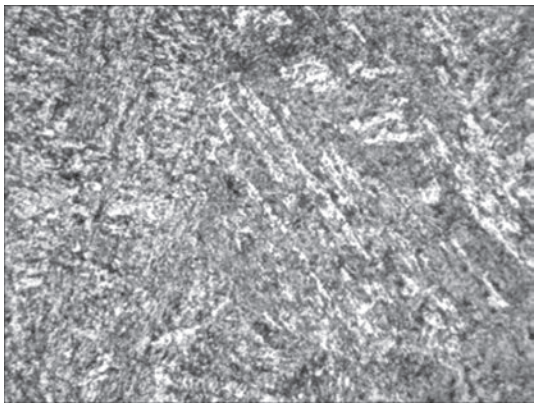

Figure 5. Initial bainite microstructure (×500) of 15Kh2NMFA steel samples

after two layers of anticorrosion surfacing for different technological modes are summarized in Table 6.

Derived calculation data on formation of bainite-martensite microstructure of 15Kh2NMFA steel, as a result of RV anticorrosion surfacing, agree quite well with published results [9, 20, 21].

Change of microstructural phase composition leads to a change of mechanical properties in HAZ of RV base material. The yield limit of each microstructural phase was determined, depending on chemical composition and temperature, based on the parametric regression equations [16].

The stress-strain state of material in RV surfaced zone was modeled using the thermo-viscoplasticity

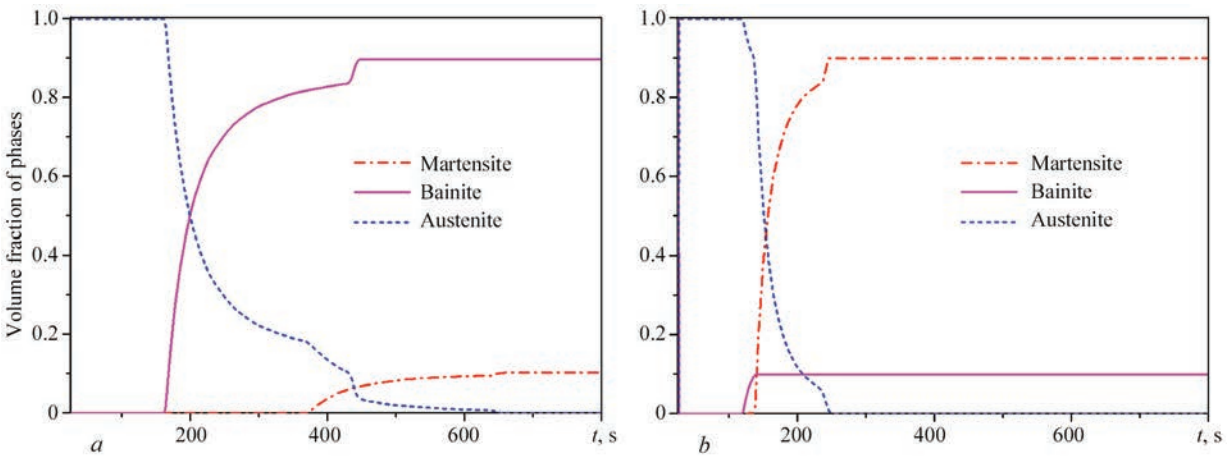

Figure 6. Results of prediction of the kinetics of austenite decomposition in HAZ metal at arc surfacing with strip electrode (b = = 60 mm) with preheating up to 250 (*a*), 150 (*b*) °C

Table 6. Results of calculation of microstructural phase composition in the HAZ of RV base material (15Kh2NMFA steel) for different technological modes of surfacing

Technological mode	Calculated data acc. to TKD, %	
	Martensite	Bainite
b = 15 mm (manual surfacing), T_{pr} = 250 °C, w = 8–11 °C/s	90	10
b = 40 mm, T_{pr} = 250 °C, w = 4–5 °C/s	70–90	10–30
b = 60 mm, T_{pr} = 250 °C, w = 3–4 °C/s	15	85
b = 60 m, T_{pr} = 150 °C, w = 5–7 °C/s	90	10

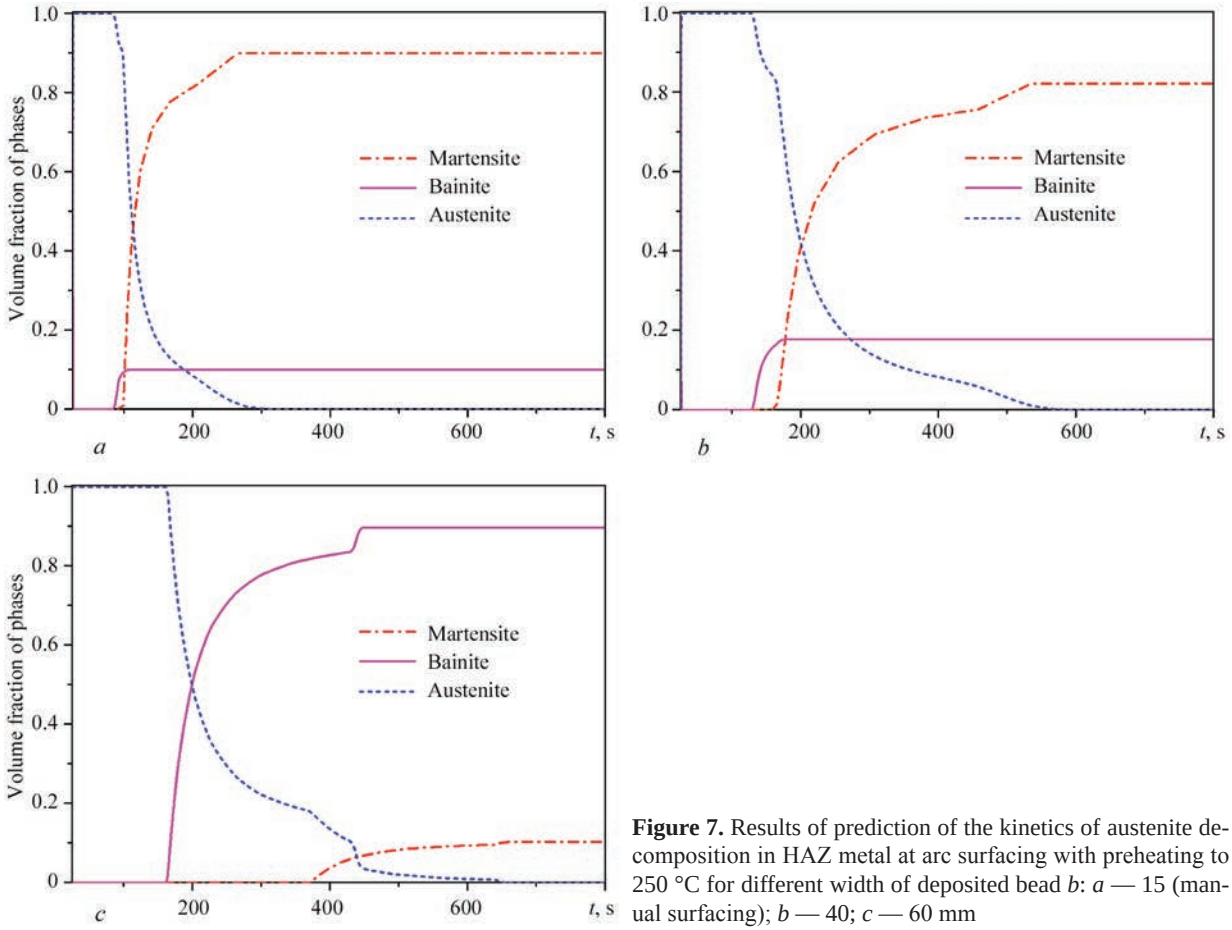

Figure 7. Results of prediction of the kinetics of austenite decomposition in HAZ metal at arc surfacing with preheating to 250 °C for different width of deposited bead *b*: *a* — 15 (manual surfacing); *b* — 40; *c* — 60 mm

model [22], for which the solution of the fundamental equations was derived by the finite element method.

Obtained were the results for residual stresses, allowing for microstructural phase transformations, based on application of experimental TKD at different technological modes of arc surfacing. Allowing for microstructural transformations and periodicity (in the transverse direction) of bead deposition on RV surface leads to nonuniform distribution of RS, appearance of compressed zones in base metal HAZ, and also influences the quantitative value of stresses. Figures 8–10 show the distribution of RS circumferential $\sigma_{\beta\beta}$ and axial σ_{zz} components in characteristic sections 1–1, 2–2.

Comparing calculation results at different widths of the deposited bead *b* = 15, 40, 60 mm (Figure 9, *a*, *b*) it was established that after two layers of deposition for all the cases of bead width, compressive circumferential RS of up to (–300– –600 MPa) were obtained in section 1–1 in base material HAZ; and the width of the compressive stress zone is equal to the depth of HAZ in the base material, while in section 2–2 we have tensile circumferential RS of up to 600 MPa in the HAZ.

After manual arc surfacing (*b* = 15 mm), the maximum value of tensile circumferential RS is up to 750 MPa, HAZ depth is up to 7 mm and the depth of

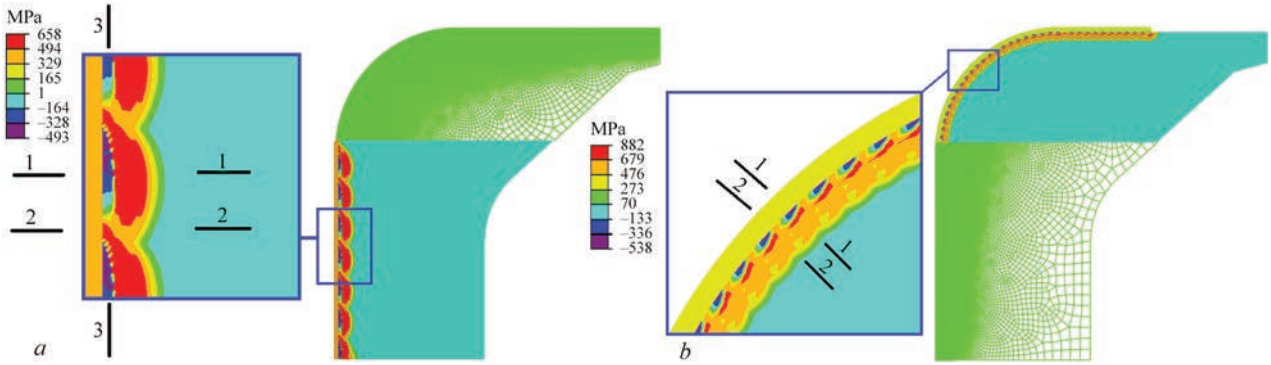

Figure 8. Distribution of circumferential RS $\sigma_{\beta\beta}$ in the cross-section of RV surfaced zone: *a* — for automatic arc surfacing with strip electrodes; *b* — for manual coated electrode arc surfacing

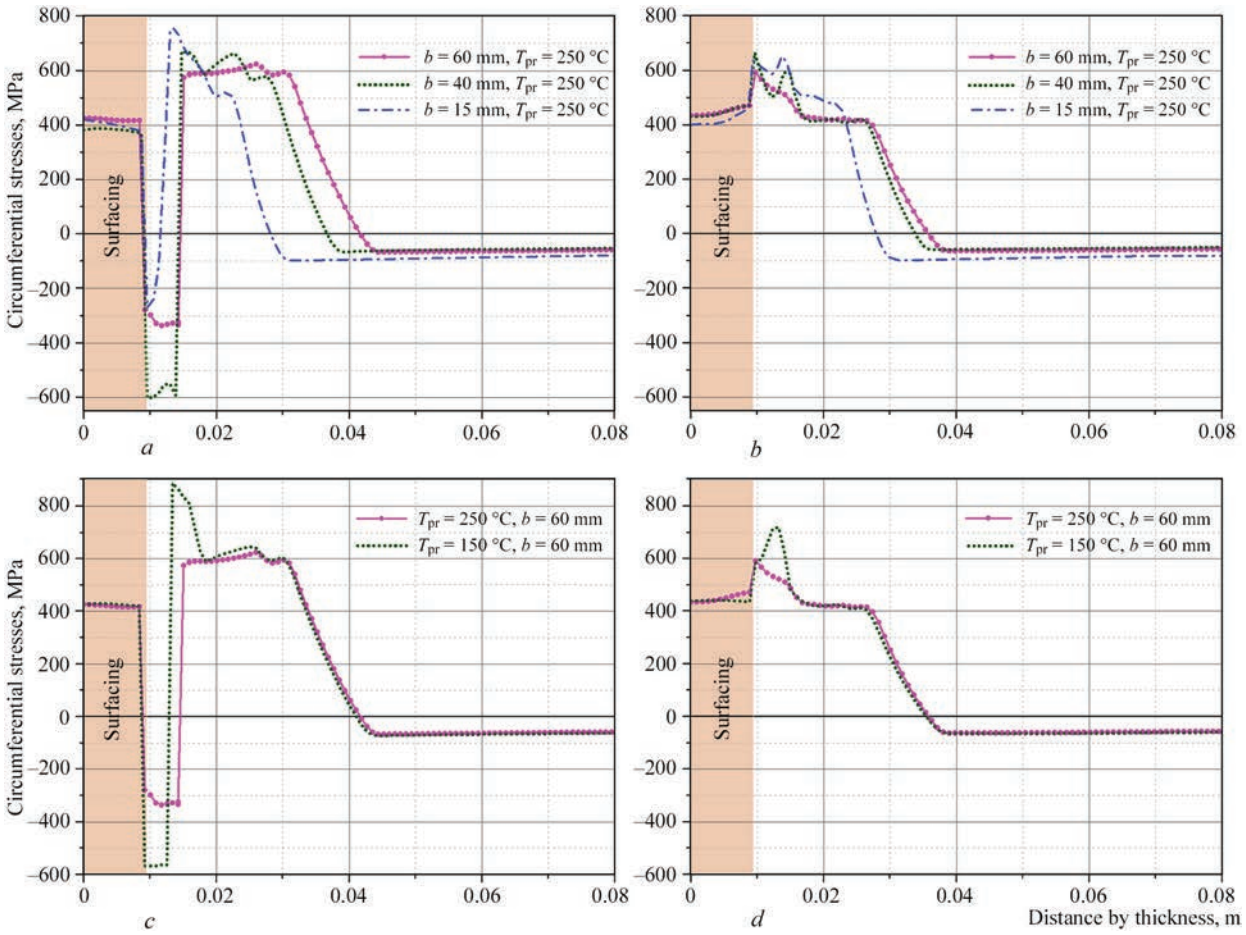

Figure 9. Distribution of circumferential RS $\sigma_{\beta\beta}$ by RV thickness after surfacing. Variation of bead width: *a* — section 1–1; *b* — 2–2. Variation of preheating temperature: *c* — section 1–1; *d* — 2–2

tensile stress zone is up to 28 mm from the deposition surface.

At surfacing with strip electrode at bead width b = 60 mm, the depth of base material HAZ is much greater and is equal up to 10 mm, at b = 40 mm it is equal up to 9 mm, the depth of tensile stress zone is equal up to 36 mm (section 2–2) — 42 mm (section 1–1) and 34 mm (section 2–2) — 36 mm (section 1–1), respectively, from the deposition surface. Maximum tensile circumferential RS for both the values of strip electrode width are close in value (600–650 MPa).

For different temperature of preheating and concurrent heating at surfacing with strip electrodes of width b = 60 mm it was found (Figure 9, *c*, *d*) that after surfacing at preheating temperature of 150 °C compressive circumferential RS of up to –570 MPa form in section 1-1 of base material, HAZ depth in base material is up to 8 mm, while at preheating temperature of 250 °C lower compressive RS — on up to –330 MPa level were obtained, but in a wider zone of base material HAZ, of up to 10 mm. Tensile circumferential RS in base material in the case of application of electrode of width b = 60 mm at preheating temperature of 150 °C locally reach the value of 840 MPa, at the temperature of 250 °C they do not exceed 600 MPa, while the depth of tensile stress zone reaches 42 mm from the deposition surface.

As regards axial component σ_{zz}, Figure 10 shows RS distribution after surfacing by the thickness RV cylindrical part in characteristic sections 1–1, 2–2, depending on the width of strip electrode and preheating temperature. Base material HAZ in RV cylindrical part has compressive RS (up to –400– –825) MPa in section 1–1, up to (–30– –200) MPa in section 2–2. Magnitude of tensile RS in the base material, allowing for microstructural transformations, is equal up to (500–620 MPa) in section 1–1 and up to (250–300 MPa) in section 2–2.

At modeling of the technological process of general (furnace) heat treatment (HT) the high-temperature tempering mode at the temperature of 650 °C for up to 20 h was specified. Stress relaxation was modeled, using the function of temperature creep of material, which in [23] was determined based on available experimental data for 15Kh2NMFA steel [9]. In particular, calculation of creep strains by the finite element method was performed using the equation correlating the rate of equivalent creep strain $d\varepsilon_{eq}^{c}$ with stress intensity σ_i in the form of Norton–Bailey law [24]:

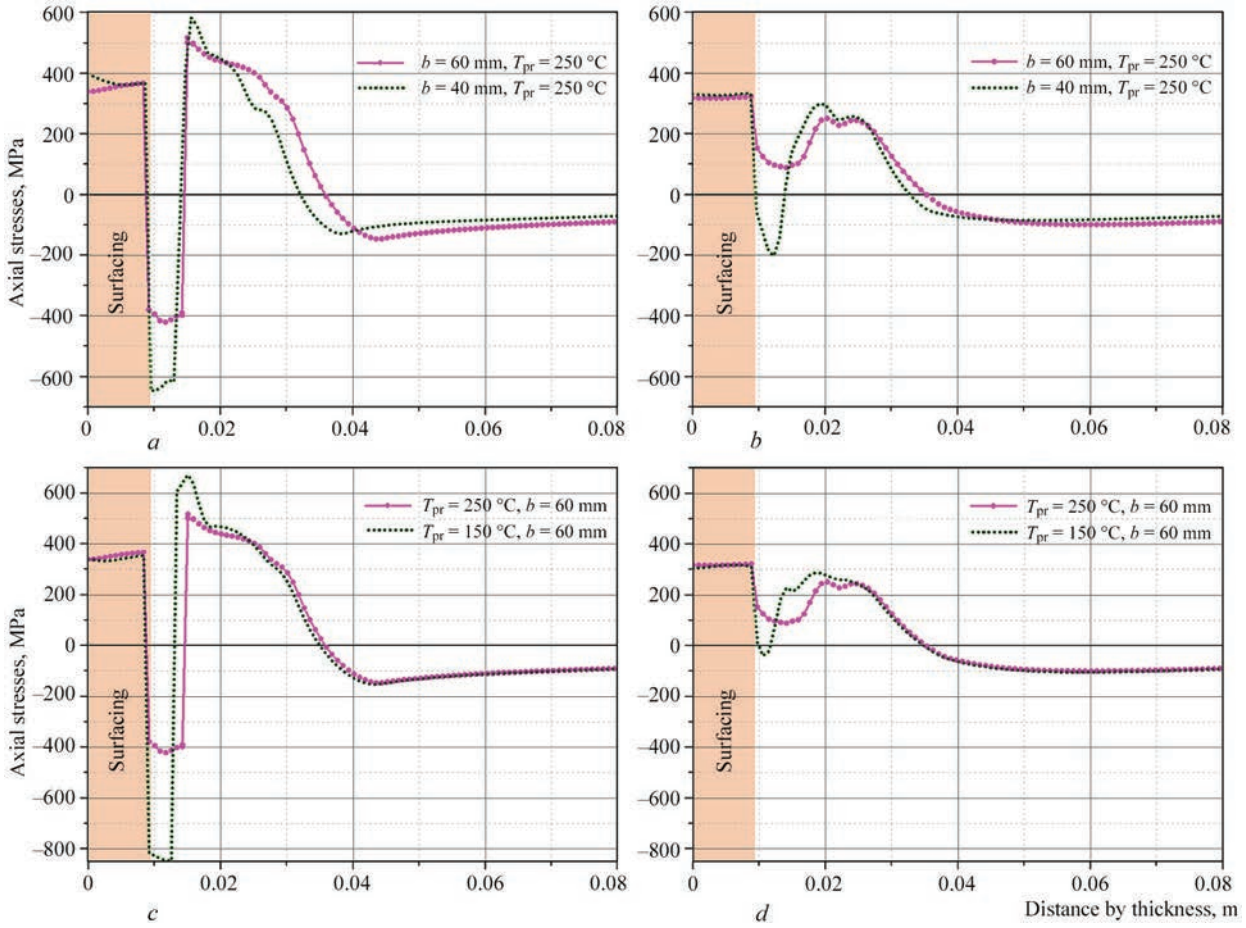

Figure 10. Distribution of axial RS σ_{zz} by RV thickness after surfacing. Variation of bead width: *a* — section 1–1; *b* — 2–2. Variation of preheating temperatures: *c* — section 1–1; *d* — 2–2

$$d\varepsilon_{eq}^{c} = A\sigma_i^n dt, \quad (5)$$

where A, n are the material constants, taking into account [9, 23] for 15Kh2NMFA steel $A = 0.17 \cdot 10^{-20}$(1/(MPa^6·s), $n = 6$.

HT by high-temperature tempering mode markedly lowers the level of residual stresses in RV base material, caused by anticorrosion surfacing. Figures 11–15 give the distributions of the circumferential and axial components of residual stresses by RV thickness after surfacing and HT performance for different technological modes. Tensile stresses on the level of austenitic material yield limit (up to 400 MPa) remain in the austenitic deposit material, because of the difference from the base material in the coefficients of temperature expansion.

Comparison of the results on circumferential RS, obtained by modeling the HT by the high-temperature tempering mode (T = 650 °C, 20 h soaking) at different width of the deposited beads and preheating temperature T_{pr} = 250 °C at surfacing showed (Figure 11, *a*, *b*) that manual arc surfacing with coated electrodes (b = 15 mm), compressive residual stresses of up to –325 MPa were obtained in base material HAZ. At automatic surfacing with strip electrode of width b = 40 mm a zone of compressive stresses of up to –330 MPa (section 2–2) and up to –500 MPa (section 1–1) was obtained in base material HAZ; at b = 60 mm the compressive stress zone (–200 MPa) (section 1–1) and the zone of tensile stresses on the level of 50 MPa (section 2–2) was formed in base material HAZ. Maximum value of tensile circumferential RS in the base material is not more than 170 MPa.

The level of circumferential residual stresses in the compression zone after HT by the mode of high-temperature tempering at a lower preheating temperature, T_{pr} = 150 °C, at surfacing is higher than that of stresses at T_{pr} = 250 °C, due to formation of a greater fraction of martensite. At automatic surfacing with strip electrodes of width b = 60 mm at preheating temperature T_{pr} = 150 °C the maximum compressive circumferential stresses can be up to (–370– –450 °C) MPa, width of the compressive zone can reach 3 mm (section 2–2) — 7 mm (section 1–1) of base material, and the depth of tensile stress zone almost does not change: up to 35 mm (section 2–2) and up to 42 mm (section 1–1) from the deposit surface (Figure 11, *c*, *d*).

Figure 12 presents the distribution of RS axial component σ_{zz} by the thickness of RV cylindrical part in characteristic sections 1–1, 2–2 after surfacing and

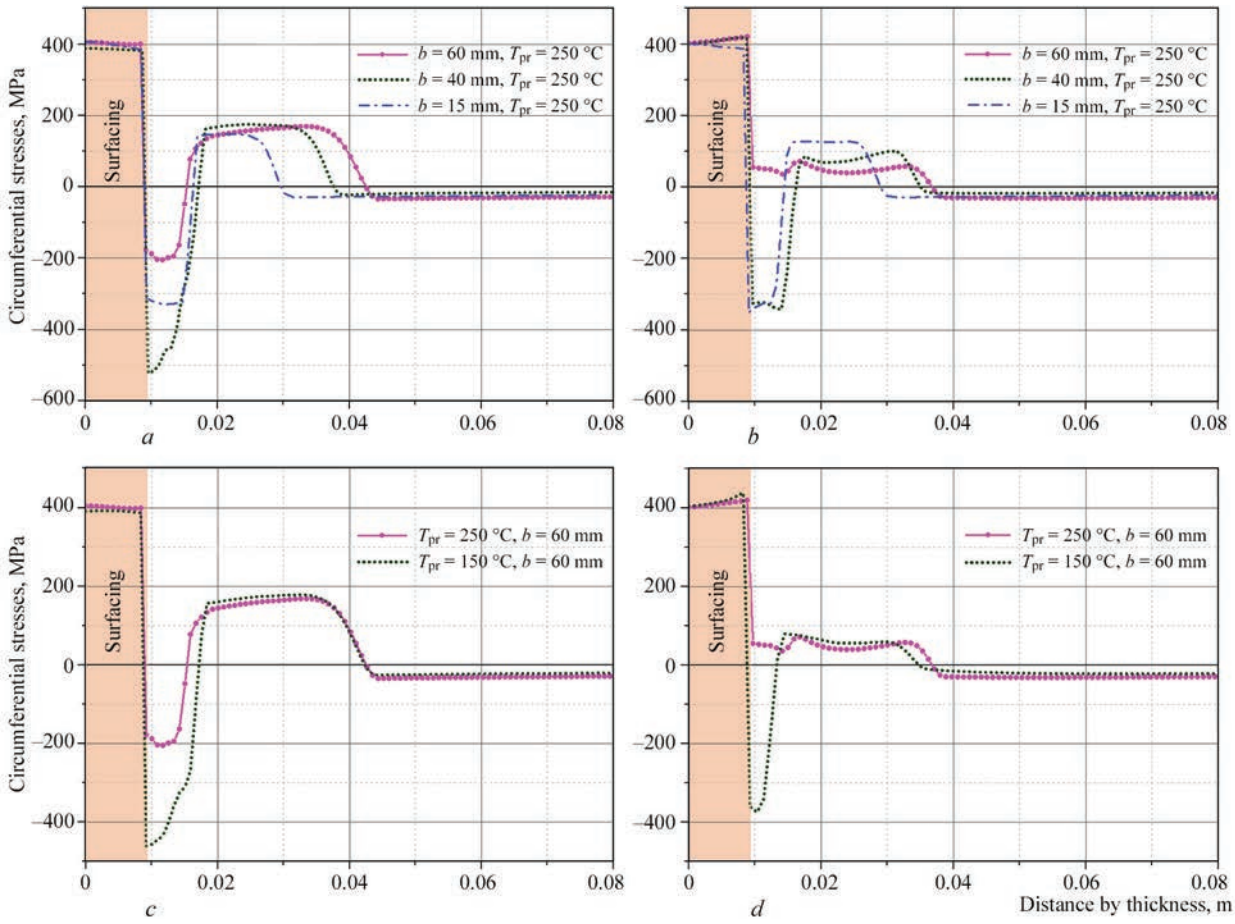

Figure 11. Distribution of circumferential RS $\sigma_{\beta\beta}$ by RV thickness after surfacing and HT (T = 650 °C, 20 h soaking). Variation of bead width: *a* — section 1–1, *b* — 2–2. Variation of preheating temperature: *c* — section 1–1; *d* — 2–2

HT by high-temperature tempering mode. The magnitude of compressive axial residual stresses, allowing for microstructural transformations in the HAZ, reaches (–220– –550) MPa in section 1–1, and (–50– –500) MPa in section 2–2. Maximum value of tensile axial residual stresses in base material does not exceed (100–120) MPa (section 1–1).

Nonuniformity of RS distribution (Figure 8, Figure 13) after surfacing (T_{pr} = 250 °C) and HT (T = 650 °C, soaking for 20 h) in the transverse direction of bead deposition (section 3-3), at 12 mm depth for the deposit surface) is represented by periodicity of values of circumferential RS from –200 to 50 MPa (strip electrode width b = 60 mm) and from –570 to 310 MPa (strip electrode width b = 40 mm). For the case of manual arc surfacing (b = 15 mm) we have an almost uniform compression zone of circumferential RS on the level of –350 MPa and slight periodicity of distribution of axial RS from –420 to –350 MPa. Axial residual stresses in the case of surfacing by strip electrodes change from –230 to –50 MPa (b = 60 mm) and from –500 to –375 MPa (b = 40 mm).

Thus results of distribution of the circumferential and axial components of residual stresses by RV thickness and in the transverse direction of bead deposition after surfacing and HT by the mode of high-temperature tempering for different technological modes showed that reduction of preheating temperature at surfacing from 250 to 150 °C leads to the HAZ narrowing and simultaneous significant increase of the magnitudes of compressive circumferential and axial RS in base material HAZ and of the width of compressive RS zone due to increase of the volume fraction of martensite component in the final microstructure. Increase of strip electrode width at surfacing leads to greater depth of the HAZ in base material, as well as of tensile RS zone. Here, narrowing of the compressive RS zone and lowering of the magnitude of compressive RS, both circumferential and axial, in the HAZ, was established due to reduction of volume fraction of the martensite component in the final microstructure.

According to Table 2, soaking duration was varied when modeling the technological operation of HT by high-temperature tempering mode at temperature T = = 650 °C, namely 5, 10 and 20 h. The results of calculation of the distribution of circumferential residual stresses by thickness, depending on soaking duration at HT are shown in Figure 14 for the case of surfacing with strip electrode b = 60 mm and in Figure 15 for

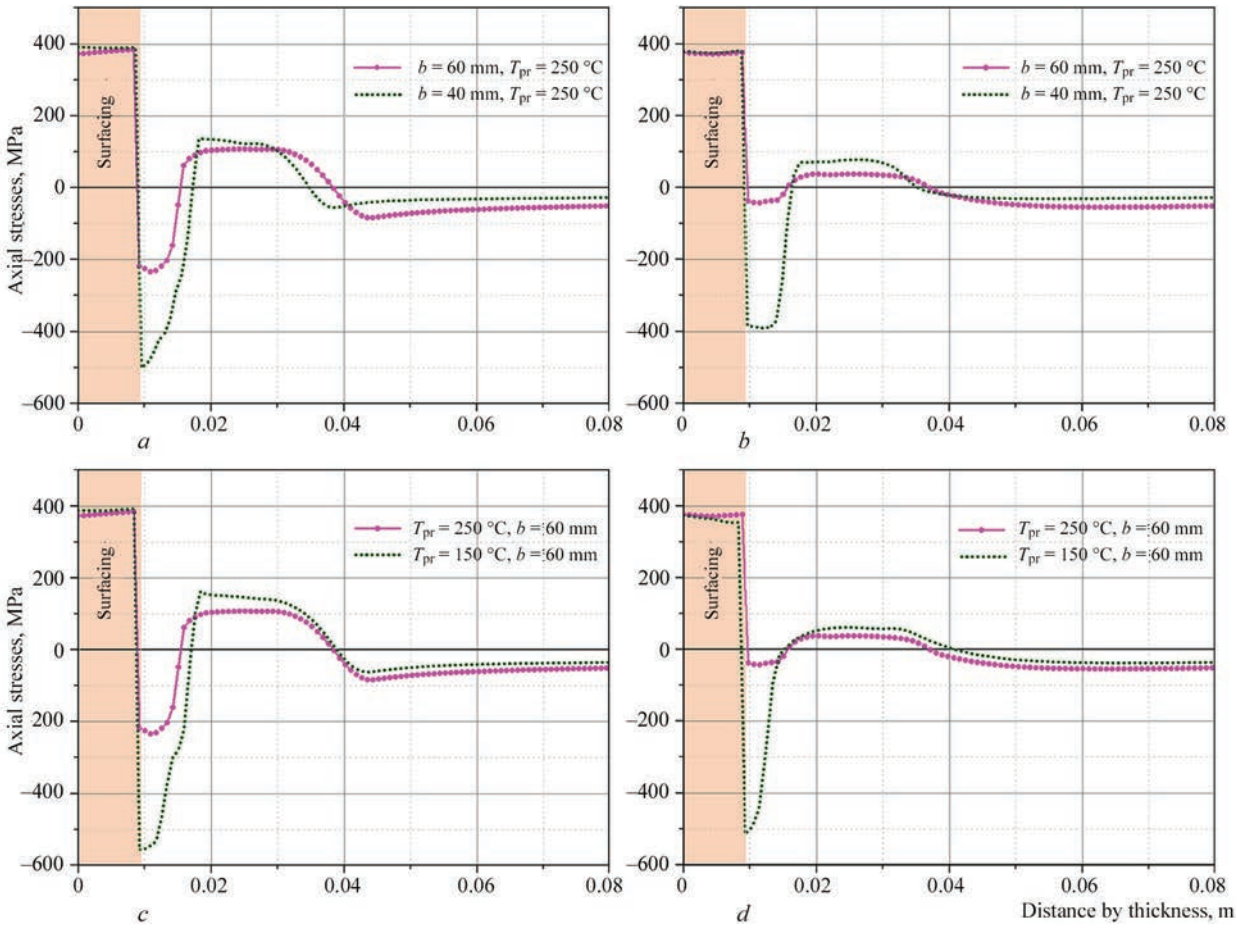

Figure 12. Distribution of axial RS σ_{zz} by RV thickness after surfacing and HT (T = 650 °C, 20 h soaking). Variation of bead width: *a* — section 1–1; *b* — 2–2. Variation of preheating temperature: *c* — section 1–1; *d* — 2–2

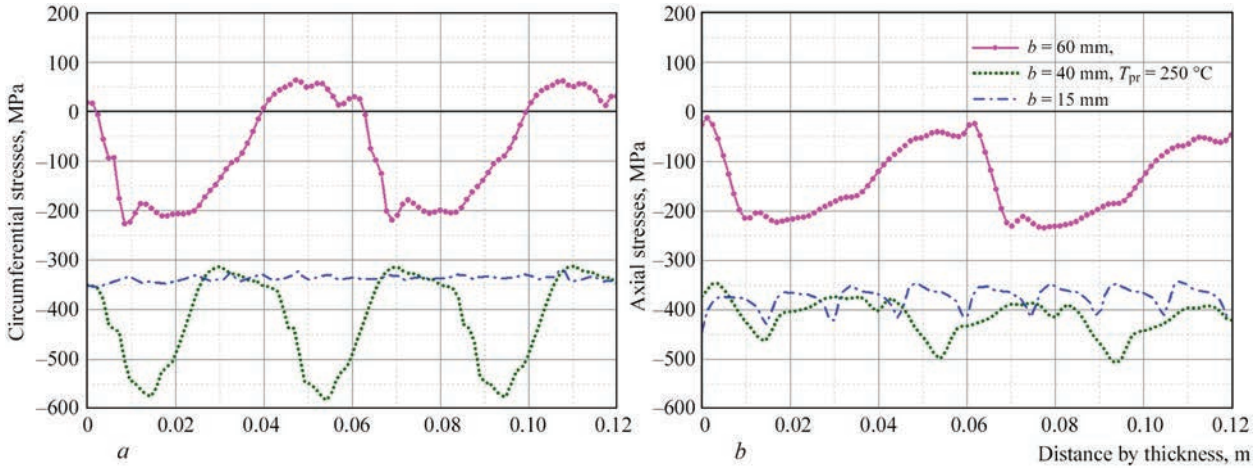

Figure 13. Distribution of circumferential $\sigma_{\beta\beta}$ (*a*) and axial σ_{zz} (*b*) RS after RV surfacing and HT (T = 650 °C, 20 h soaking) in base material HAZ in section 3–3 (in transverse direction of bead deposition, at 12 mm depth from deposit surface)

the case of manual surfacing with coated electrodes, b = 15 mm.

The results (Figure 14) show that the maximum level of tensile RS in base material after 5 h soaking at HT decreased to 220 MPa, after 10 h — to 200 MPa, and after 20 h — to 170 MPa (section 1–1). Maximum magnitudes of compressive stresses in the HAZ were also obtained at 5 h soaking duration, namely –235 MPa.

For coated electrode manual arc surfacing (Figure 15), lowering of the maximum level of tensile RS in base material to 200 MPa was obtained at HT after 5 h soaking, to 175 MPa after 10 h, and to 150 MPa after 20 h (section 1–1). In base material HAZ lowering of maximum magnitude of compressive stresses to –330– –350 MPa was achieved at 5 h soaking duration.

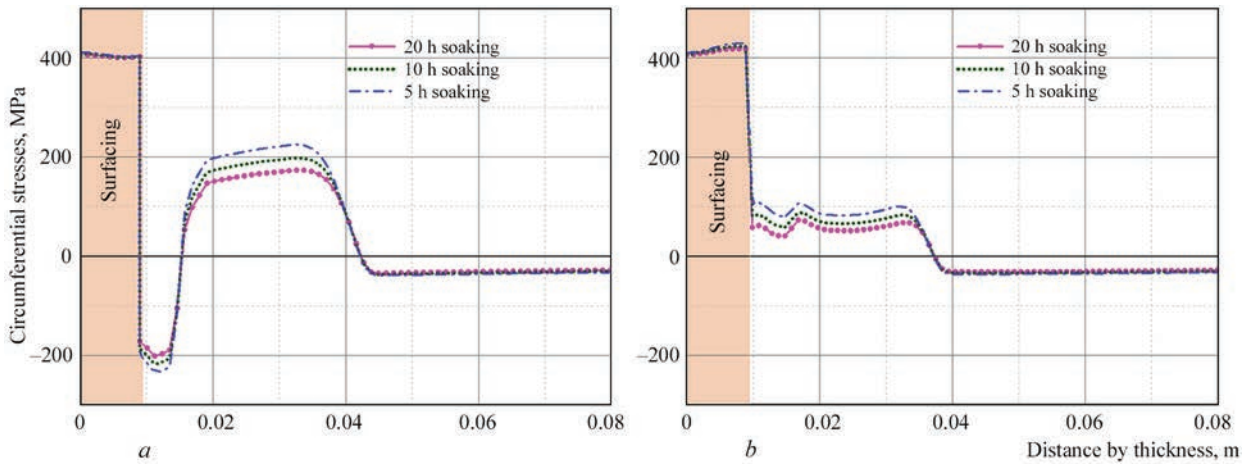

Figure 14. Distribution of circumferential RS $\sigma_{\beta\beta}$ by RV thickness for two characteristic sections at variation of heat treatment mode (soaking duration at $T = 650$ °C) for the case of submerged-arc surfacing with strip electrode $b = 60$ mm: *a* — section 1–1; *b* — section 2–2

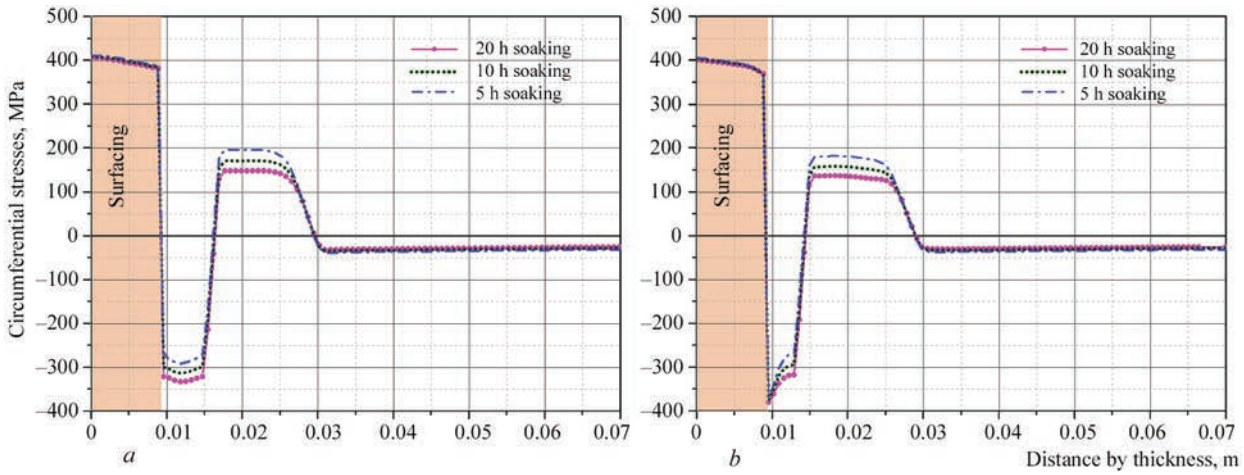

Figure 15. Distribution of circumferential RS $\sigma_{\beta\beta}$ by RV thickness in two characteristic sections at variation of heat treatment mode (soaking duration at $T = 650$ °C) for the case of manual arc surfacing with coated electrodes $b = 15$ mm: *a* — section 1–1; *b* — section 2–2

Conclusions

1. For WWER-1000 RV made from low-alloyed high-strength 15Kh2NMFA steel, on the internal surface of which an anticorrosion layer from austenitic material was deposited by two different technologies: automatic submerged-arc surfacing with strip electrodes of RV cylindrical part and manual coated electrode arc surfacing of the internal surface of the nozzles, calculated data were obtained as regards the kinetics of temperature distribution, cooling rates, FZ and HAZ dimensions and kinetics of microstructural phase transformations.

2. As a result of modeling the microstructural phase composition by the data of welding TKD for 15Kh2NMFA steel, martensite content from 15 to 90 % in base material HAZ was obtained for submerged-arc strip surfacing of RV cylindrical part, and predominant martensite content of up to 90 % for manual coated electrode arc surfacing of the internal surface of nozzle Dn850. Thus, technologies of arc surfacing with an anticorrosion layer of the internal surface, currently used in WWER-1000 RV manufacture, despite preheating up to 150–250 °C led to formation of a phase structure with high martensite content to the depth of up to 10 mm in base material HAZ.

3. A significant influence of variation of technological parameters of the surfacing and heat treatment process (strip electrode width, preheating temperature, soaking duration at heat treatment) on RS distribution in the surfaced zone of WWER-1000 RV was revealed. Analysis of the comparison of calculated RS distribution, allowing for microstructural phase transformations, showed the following main features, namely owing to the periodicity of deposition of the surfacing passes (beads) and formation of bainite-martensite microstructure, the base material HAZ develops a significant nonuniformity of RS distribution in the transverse direction of deposition and a zone of compressive stresses on the level of (–200–550) MPa of up to 7 mm width at the depth from 9 to 16 mm from the deposit surface. Then, at the depth

from 16 to 42 mm they change to tensile stresses of the maximum level of up to 170 MPa. In the austenitic deposited material tensile stresses on the level of the austenitic material yield limit (up to 400 MPa) remain even after HT, because of the difference in thermal expansion coefficients with the base material.

4. It was found that lowering of preheating temperature from 250 to 150 °C at surfacing leads to an essential increase of volume fraction of martensite component in the final microstructure and increase of the magnitude of compressive circumferential and axial RS in the HAZ, as well as to increase of the width of the compressive RS zone.

5. Increase of the strip electrode width to b = = 60 mm at surfacing leads to a significant increase of the width of the HAZ, as well as tensile RS zone in base material. Here, a lowering of the magnitude of compressive RS, both circumferential and axial in the HAZ, and reduction of the compressive RS zone was found at reduction of the volume fraction of martensite component in the final microstructure.

6. Increase of soaking duration at high-temperature annealing temperature of 650 °C promotes RS relaxation in the base material, particularly, lowering of the magnitude of maximum tensile circumferential stresses from (220–200) MPa at 5 h soaking to (170–150) MPA at 20 h soaking.

1. (2003) PNAE G-7-009–89: Equipment and pipelines of nuclear power plants. *Welding and surfacing, basic provisions.* Moscow [in Russian].
2. (1982) Welded vessel 1152.02.70.000. *Appendix to pressure vessel certificate 1152.02.70.000 D7, ZNPP, bl. 1* [in Russian].
3. Titova, T.I.,Shulgan, N.A. (2013) Improvement of quality of welded joints and deposited surfaces of NPP equipment OJSC production «Izhorskie zavody». In: *Proc. of Conf. on Ensuring the Safety of NPP with WWER*, St.-Petersburg, Gidropress [in Russian]. http://www.gidropress.podolsk.ru/files/proceedings/mntk2013/autorun/article95ru.htm
4. Iradj, Sattari-Far, Magnus, Andersson (2006) *Cladding effects on structural integrity of nuclear components.* SKI Report 2006:23, ISSN 1104-1374, ISRN SKI-R-06/23-SE.
5. Katsuyama, J., Udagawa, M., Nishikawa, H. et al. (2010) Evaluation of weld residual stress near the cladding and J-weld in reactor pressure vessel head for the assessment of PWSCC behavior. *Japan Society of Maintenology. E-J. of Advanced Maintenance*, **2**, 50–64.
6. Dupas, P., Moinereau, D. (1996) Evaluation of cladding residual stresses in clad blocks by measurements and numerical simulations. *J. de Physique IV Colloque*, **6**, 187–196.
7. Ryabtsev, I.A., Senchenkov, I.K. (2013) Theory and practice of surfacing operations. Ekotekhnologiya [in Russian].
8. Tsvitanovich, M., Postruzin, Zh., Munk, R. et al. (2011) System of ultrasonic testing of reactor vessel metal of Kudankulam NPP. In: *Proc. of Conf. on Ensuring the Safety of NPP with WWER, Podolsk, Gidropress* [in Russian]. http://www.gid-ropress.podolsk.ru/files/proceedings/mntk2011/documents/mntk2011-184.pdf
9. Margolin, B.Z., Varovin, A.Ya., Kostylyov, V.I. (2005) Determination of residual stresses in the WWER vessels after multi-run welding, surfacing and high-temperature tempering. *The Paton Welding J.*, **10**, 14–20.
10. (1978) TU 108-765–78: *Billets of steel of 15Kh2NMFA and 15Kh2NMFA-A grades for vessels and covers and other assemblies of reactor plants* [in Russian].
11. Kostylev, V.I., Margolin, B.Z. (2000) Determination of residual stress and strain fields caused by cladding and tempering of reactor pressure vessels. *Int. J. of Pressure Vessels and Piping*, **77**, 723–735.
12. (2000) *Procedure for determination of service life of nuclear reactor vessels during operation (MRK-SKhR-2000), RD EO 0353-02*, St.-Petersburg-Moscow [in Russian].
13. Makhnenko, O.V., Kostin, V.A., Zhukov, V.V., Kostenevich, E.S. (2019) Effect of cooling cycle of welding on structure-phase composition of 15Kh2NMFA steel. *The Paton Welding J.*, **9**, 8–17.
14. Hrivnak, I. (1984) *Weldability of steels*. Ed. by E.L. Makarov. Moscow, Mashinostroenie [in Russian].
15. Kasatkin, O.G., Seyffarth, P. (2002) Calculation models for evaluating mechanical properties of HAZ metal in welding low-alloyed steels. In: *Proc. of Int. Conf. on Mathematical Modeling and Information Technologies in Welding and Related Processes.* Kiev, 103–106.
16. Kasatkin, O.G. (1990) Mathematical modeling of relations composition-properties of welded joints and development of calculation and experimental system for optimization of main technological factors for welding of low-alloyed structural steels*: Syn. of Thesis for Dr. of Tech. Sci. Degree.* Kiev, PWI [in Russian].
17. Lobanov, L.M., Kostin, V.A., Makhnenko, O.V. et al. (2020) Forecasting of structural transformations in heat affected zone steel of 15KH2NMFA at anti-corrosion cladding. *Problems of Atomic Science and Technology*, 126(**2**), 89–96.
18. Gurovich, B.A., Kuleshova, E.A., Fedotova S.V. (2011) Influence of chemical composition and structural parameters of steels of WWER reactor vessels on susceptibility to embrittlement caused by formation of grain boundary segregations including the conditions characteristic for long-term operation of power plants. In: *Proc. of 7th Int. Sci.-Techn.Conf. on Ensuring the Safety of NPP with WWER,* Podolsk, Gidropress. http://www.gidropress.podolsk.ru/files/proceedings/mntk2011/autorun/article151-ru.htm
19. Frolov, A.S. (2013) Phase-structural state and service characteristics of new steel compositions for reactor vessels of higher power and service life*: Syn. of Thesis for Cand. of Tech. Sci. Degree*, Moscow, NRC Kurchatov Institute [in Russian].
20. Teplukhina, I.V., Golod, V.M., Tsvetkov, A.S. (2018) CCT diagram plotting based on the numerical analysis of dilatometric tests results. *Letters on Materials*, **8**(1), 37–41.
21. Soloviov, I.V., Kornienko, O.Yu., Zhilyakov, A.Yu., Belorusets, A.M. (2017) Examination of kinetics of overcooled austenite decomposition of 15Kh2NMFA steel during continuous cooling. In: *Proc. of 18th Int. Sci.-Techn. Ural School-Seminar of Metallurgists-Junior Scientists* (Ekaterinburg, 21-23 November 2017), UrFU, 250–252.
22. Makhnenko, V.I. (1976) *Calculation methods of investigation of welding stresses and strains.* Kiev, Naukova Dumka [in Russian].
23. Makhnenko, V.I. (2006) *Safe service life of welded joints and assemblies of modern structures*. Kiev, Naukova Dumka [in Russian].
24. Betton, J. (2008) *Creep Mechanics.* 3-rd ed. Springer, Germany, XVI.

Received 02.11.2020